Anal. Chem. **2000,** *72,* 2987−2994

Converting Spatial to Pseudotemporal Resolution in Laser Plasma Analysis by Simultaneous Multifiber Spectroscopy

Valery Bulatov, Rivie Krasniker, and Israel Schechter*

Department of Chemistry, Technion-Israel Institute of Technology, Haifa 32000, Israel

Traditional chemical analysis based on laser plasma spectroscopy (LPS) requires time-gated detectors, to avoid the initial signal from the hot plasma. These detectors are expensive and often need to be cooled and protected against vapor condensation. We suggest a low-cost setup that may replace these gated detectors, while maintaining acceptable analytical performance. The proposed setup is a result of investigation of plasma-front propagation in LPS analysis. It is known that the LPS plasma propagation is similar to the shock wave propagation after a strong explosion in the atmosphere. We found that the propagation of the plasma fits well the Sedov blast wave theory, providing a good agreement between the theoretical and experimental figures. A proper observation geometry, which is perpendicular to the plasma expansion vector, enables converting spatial to temporal resolution. We take advantage of the fact that the plasma reaches a given distance above the analyzed surface at a certain time delay. Therefore, a single optical fiber, positioned at a well-defined geometry, can provide spectral information corresponding to a certain time delay. A multifiber imaging spectrometer provides information corresponding to a series of delay times, which is adequate for analysis of a variety of matrixes. It was found that the performance of the nongated detector observing a narrow solid angle is similar to that of a gated one observing the whole plasma. For one particular example, observing the plasma from a distance of 4.5 mm is equivalent to a delay of 4 μs and integration time of 2 μs. The ratio of spectral lines of two elements was investigated using the spatially resolved (nongated) setup, and it was found that this mode is advantageous when internal calibration is applied. It was concluded that sensitive LPS analyses can be carried out by less expensive (nongated) detectors.

Laser plasma spectroscopy, also known as laser-induced breakdown spectroscopy (LIBS), is a simple and well-established analytical method. It is based on analysis of atomic emissions from laser-induced plasma, obtained by focusing a pulsed laser beam onto the sample. Considerable research efforts and interest have been recently devoted to LPS analysis, mainly due to its potential in direct analysis of solids and of particulate materials,[1−21] including analysis of surface impurities,[1] surface spectral imaging,[2,3] aerosols, and hydrosols.[4−7] Since analytical results are obtained within seconds and no sample preparation is needed, this technique is often considered for environmental monitoring[8−18] and for industrial process control.[19−21] Although moderate relative detection limits were reported (in the ppm range), the absolute sensitivity of this method is high (in the nanogram range), allowing for numerous applications.[18,22]

A typical LPS setup includes a laser, a spectrometer and a gateable detection system, such as an intensified CCD camera or an intensified photodiode array. The temporal gating is essential, due to the high initial plasma temperature (ca. 50 000 C) which causes an intensive blackbody radiation component, noise of various origins, and an abundance of unstable spectral lines corresponding to ionic species. Moreover, when temporal resolution is available, it can be used for optimizing the signal-to-noise ratio, which is a function of delay and integration times.

Most recent LPS studies, which are related to the current report, deal with the introduction of spatial resolution and its various effects. Spatial versus spectral resolution trade off is a

(1) Franzke, D.; Kloss, H.; Wokaun, A. *Appl. Spectrosc.* **1992**, *46*, 587−592.
(2) Hakkinen, H. J.; Korppi-Tommola, J. E. I. *Appl. Spectrosc.* **1995**, *49*, 1721.
(3) Romero, D.; Laserna, J. J. *Anal. Chem.* **1997**, *69*, 2871−2876.
(4) Neuhauser, R. E.; Panne, U.; Niessner, R.; Petricci, G. A.; Cavali, P.; Omeneto, N. *Anal. Chim. Acta* **1997**, *346*, 37−48.
(5) Poulan, D. E.; Alexander, D. R. *Appl. Spectrosc.* **1995**, *49*, 569−579.
(6) Schechter, I. *Anal. Sci. Technol.* **1995**, *8*, 779.
(7) Haisch, C.; Liermann, J.; Panne, U.; Niessner, R. *Anal. Chim. Acta* **1997**, *346*, 23−35.
(8) Anglos, D.; Couris, S.; Fotakis, C. *Appl. Spectrosc.* **1997**, *51*, 1025.
(9) Gornishkin, I. B.; Kim, J. E.; Smith, B. W.; Baker, S. A.; Winefordner, J. D. *Appl. Spectrosc.* **1997**, *51*, 1055.
(10) Jamamoto, K. J.; Cremers, D. A.; Ferris, M. J.; Foster, L. E. *Appl. Spectrosc.* **1996**, *50*, 222.
(11) Pakhomov, A. V.; Nichols, W.; Borysow, J. *Appl. Spectrosc.*, **1996**, *50*, 880.
(12) Marquardt, B. J.; Goode, S. R.; Angel, S. M. *Anal. Chem.*, **1996**, *68*, 977.
(13) Nakamura, S.; Ito, Y.; Sone, K.; Hiraga, H.; Kaneko, K. *Anal. Chem.* **1996**, *68*, 2981.
(14) Vadillo, J. M.; Laserna, J. J. *Talanta* **1996**, *43*, 1149−1154.
(15) Jensen, L. C.; Langford, S. C.; Dickinson, J. T.; Addleman, R. S. *Spectrochim.* Acta **1995**, *50B*, 1501−1519.
(16) Howden, S.; Schneider, Ch.; Grosser, Z. *At. Spectrosc.* **1996**, *17*, 171−175.
(17) Eppler, A. S.; Cremers, D. A.; Hickmott, D. D.; Ferris, M. J.; Koskelo, A. C. *Appl. Spectrosc.* **1996**, *50*, 1175−1181.
(18) Wisbrun, R.; Schechter, I.; Niessner, R.; Schröder, H.; Kompa, K. L. *Anal. Chem.* **1994**, *66*, 2964.
(19) Kim, D. E.; Yoo, K. J.; Park, H. K.; Oh, K. J.; Kim, D. W. *Appl. Spectrosc.* **1997**, *51*, 22.
(20) Ernst, W. E.; Farson, D. F.; Sames, D. J. *Appl. Spectrosc.* **1996**, *50*, 306.
(21) Zhang, H.; Singh, J. P.; Yueh, F. Y.; Cook, R. L. *Appl. Spectrosc.* **1995**, *49*, 1617.
(22) Omeneto, N.; Petrucci, G. A.; Cavali, P.; Winefordner, J. D. *Fresenius' J. Anal. Chem.* **1996**, *355*, 878−882.

10.1021/ac0001737 CCC: $19.00
Published on Web 06/01/2000

must, due to technical reasons. A combination of spatial (2D) and single-wavelength resolution was obtained by fast photographic techniques.[23,24] Application of tunable filters in front of the CCD camera provided wavelength resolution; however, full spectra from single shots could not be obtained this way. Spatial (2D) and multiwavelength resolutions were recently obtained with a new setup, providing full spectrum at each CCD pixel.[25] This setup, consisting of a Fourier transform spectrometer coupled to a cooled CCD detector, allowed for mapping of certain elements in the plasma. However, due to the nature of this spectrometer, the results must be averaged over many laser shots.

Spatial (1D) combined with spectral resolution was achieved by imaging spectrometers and applied to LPS analysis. A very useful experimental setup, based on an optical imaging spectrometer, was originally designed by Olesik and Hieftje more than 10 years ago.[26] A similar setup was recently applied,[19,27−29] by focusing the plasma image onto the entrance slit of an imaging spectrometer.

One of the current drawbacks of the LPS technique is the high cost of the experimental setup. The most expensive component is the gateable detector (intensified CCD or PDA). For this reason, time-integrated methods, which do not require gateable detectors, are of considerable importance for many applications.[10,28−31] (The cost of a CCD detector is only a fraction of that of an ICCD.) For example, a low-cost detector could be successfully applied in LPS instruments designed for environmental applications.[10] Mao et al. investigated the influence of laser plasma propagation on the temperature and emission spatial profile, by using a low-cost time-integrated detector.[28]

Both spectral and spatial resolution from *single* laser shots was recently achieved using a multifiber imaging spectrometer.[24,32] This setup provided excellent spectral data, however, the spatial resolution was limited by the number of optical fibers applied. This setup is the basis of the current report.

In this study we report a simple spectroscopic setup which provides both spatial and high spectral resolutions, at time-integrated mode. The spatial resolution is utilized for effective temporal gating, thus demonstrating the possibility of avoiding a gateable detector. In other words, we show, for the first time, how spatial resolution can be converted to temporal resolution, thus avoiding the expensive intensified detector. The sensitivity of the proposed setup is adequate for acquisition of multidimensional information from single laser shots. Its performance is exemplified by analysis of brass samples. The spatial distribution of the plasma as a function of analyte concentration is discussed. Results on the dynamics of the spatial propagation of the plasma plume as a function of laser-pulse energy and its surface density and sample composition are also provided. The performance of the well-known internal calibration technique, which is based on the ratio of two elemental lines, was examined by the proposed setup. The later is expected to result in somewhat better calibrations than those obtained by gated measurements.

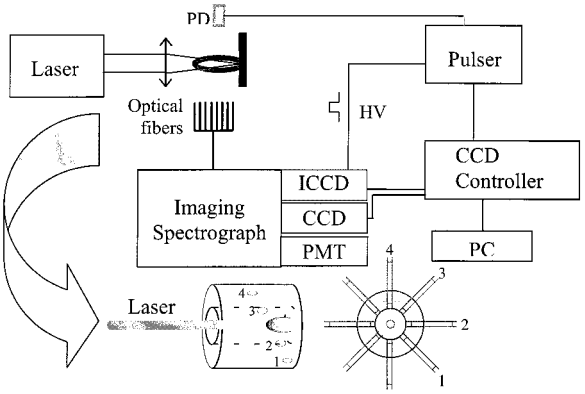

Figure 1. Experimental setup providing spatial plasma resolution, with high spectral resolution, from single laser shots.

EXPERIMENTAL SECTION

Experimental Setup. A new setup was design for nongated simultaneous spectral acquisition at various locations along the plasma plume, with high spectral resolution. Its sensitivity allowed for single-shot measurements. The experimental arrangement is similar to the one recently reported[32] and is shown in Figure 1. Plasma excitation was carried out with a Q-switched Nd:YAG laser (Continuum, Powerlite-8010, Santa Clara, CA) operated at its fundamental wavelength (1060 nm), at a low (1 Hz) repetition rate. This repetition rate eliminates effects due to aerosol production, resulting from the laser-induced shock wave.[18] The pulse energy was attenuated to 400 mJ, and the duration of the pulses was 7 ns. The laser beam was focused with a planoconvex quartz lens of $f = 250$ mm. The focal length was relatively short in order to avoid breakdown in front of the observation region. The solid samples were positioned 50 mm in front of the focal point, such that sensitivity to crater formation was minimized, while maximizing the interaction area. Under these conditions the irradiance was 2.25×10^9 W cm^{-2} (400 mJ, 7 ns). When the plasma plume propagation was investigated, this position was varied in the range 20−60 mm in front of the focal point.

The spectrally resolved plasma light was monitored in three different modes: (a) spatially resolved, using a CCD; (b) temporally resolved, using an ICCD detector; (c) continuous temporal monitoring, using a photomultiplier detector. All the three alternative modes are schematically shown in Figure 1.

Plasma emission was simultaneously inspected through an eighth-furcated optical fiber bundle (fused silica, 200 μm each). This arrangement is schematically shown in Figure 1. Seven fiber-ends were placed along the axis of the plasma plume, 1.5 mm apart. The optical geometry of the fiber housing and the sample holder ensured a small collection angle, resulting in a spatial resolution of less than 1 mm.

The eighth fiber of the above bundle was used for inspection of the whole plasma plume, with no spatial resolution. It was placed 5 cm apart from the sample, at an angle of 15° to the laser beam direction. The measurements through this fiber were gated at a

(23) Castle, B. C.; Visser, K.; Smith, B. W.; Winefordner, J. D. *Appl. Spectrosc.* **1997**, *51*, 1017−1024.
(24) Bulatov, V.; Schechter, I. *Internet J. Chem.* **1998**, *1*, 8.
(25) Bulatov, V.; Xu, L.; Schechter, I. *Anal. Chem.* **1996**, *68*, 2966−2973.
(26) Olesik, J. W.; Hieftje, G. M. *Anal. Chem.* **1985**, 57, 2049.
(27) Vadillo, J. M.; Milan, M.; Laserna, J. J. *Fresenius' J. Anal. Chem.* **1996**, *355*, 10−15.
(28) Mao, X. L.; Shannon, M. A.; Fernandez, A. J.; Russo, R. E. *Appl. Spectrosc.* **1995**, *49*, 1054−1062.
(29) Iida, Y.; Morikawa, H.; Tsuge, A.; Uwamino, Y.; Ishizuka, T. *Anal. Sci.* **1991**, *7*, 61−64.
(30) Nordstrom, R. J. *Appl. Spectrosc.* **1995**, *49*, 1490−1499.
(31) Lee, Y.-Ill.; Sawan, S. P.; Thiem, T. L.; Teng, Y.-Y.; Sneddon, J. *Appl. Spectrosc.* **1992**, *46*, 436−441.
(32) Bulatov, V.; Krasniker, R.; Schechter, I. *Anal. Chem.* **1998**, *70*, 5302−5311.

given delay and integration time. Therefore, the data collected by this fiber are similar to those obtained in traditional LPS analysis. These results were used for comparison with the nongated figures from the other 7 fibers.

The above optical fiber setup provided two different measurement schemes: (a) spatially resolved data (with no temporal gating) using the 7 fibers positioned perpendicular to the laser beam; (b) temporally resolved data (with no spatial resolution), using the single (8th) fiber positioned to view the whole plasma.

The other end of the bundle was coupled into an imaging spectrometer (SpectraPro-500i, Acton Research Corp., Acton, MS), through a special imaging interface. A 1200 g/mm grating was used, resulting in a spectral resolution better than 0.2 nm, over a range of 38 nm. In the gated experiments, spectra were recorded by an intensified, thermoelectrically cooled, fiber coupled CCD camera (Princeton Instruments, Trenton, NJ). The long CCD axis (1352 pixels, 1024 of them covered by a 25 mm intensifier) was used for recording the spectra, while the short axis (350 pixels) was logically divided into strips, each devoted to an individual optical fiber. The CCD and the spectrometer were aligned such that no cross-talk between the fibers was observed. Most pixels corresponding to the same wavelength and originating from the same fiber (ca. 15) were logically bined, to increase sensitivity.

Data Acquisition. In the nongated experiments, the laser was operated at 1 Hz, while the shutter of the *nongated* CCD detector was opened for 1 s. This way, 10 consecutive spectra were acquired without time resolution. In the gated experiments, a small portion of the laser light was reflected onto a fast photodiode, for triggering. The later triggered a delay generator (PG-200, Princeton Instruments, Trenton, NJ), which controlled the high-voltage gating pulses supplied to the intensifier. Two series of gated experiments were carried out: In the first, a delay time of 4 μs and an integration time of 2 μs were applied, which provided a good signal-to-noise ratio together with a reasonable temporal resolution. In the second series the same delay time was applied, but the integration time was longer, 100 μs. All data were collected in single-shot mode and treated according to the previously reported scheme.[33] Finally, a proper averaging over 10 pulses was carried out.

The data acquisition and analysis were carried out using standard software packages (WinView and WinSpec by Princeton Instruments) and other specific home-written programs. All codes were written in FORTRAN 77 and compiled with MS-FORTRAN Power Station Compiler. All programs were run on a PC.

Plasma Propagation Measurements A modified setup was used for the measurements of spatial propagation of the plasma front. The CCD detector was replaced by a PMT (R938, Hamamatsu), positioned on the second output port of the spectrometer. Temporally resolved data were acquired by a single fiber positioned at various distances from the target. All measurements were performed with 200 μm entrance and exit slits. Switching from CCD-port to PMT-port was performed by rotating an internal mirror. A digital oscilloscope (LeCroy 9300), triggered by a fast-responding photodiode, acquired the resulting emission signals.

(33) Xu, L.; Bulatov, V.; Gridin, V.; Schechter, I. *Anal. Chem.* **1997**, *69*, 2103−2108.

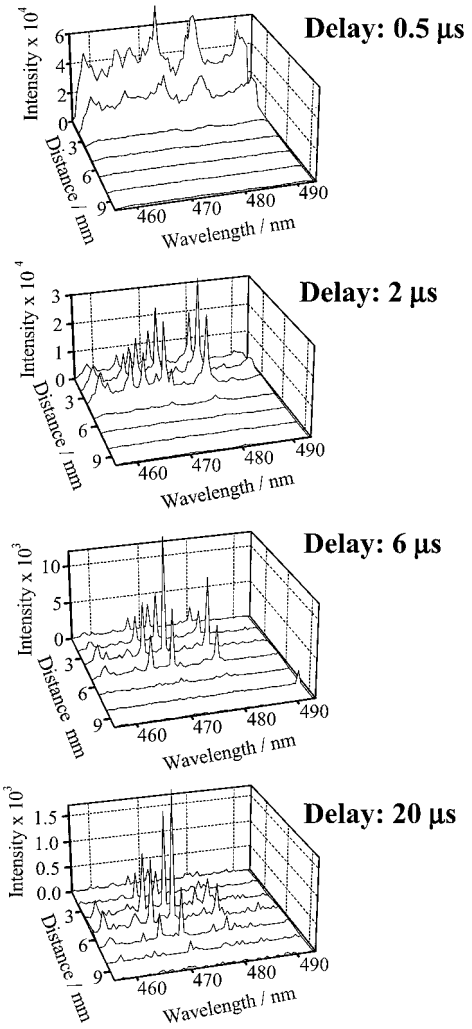

Figure 2. Spectra of brass sample vs distance acquired at several delay times. The integration time was 100 ns.

Sample Preparation. A series of brass samples were analyzed. The Zn weight concentration varied between 0% and 30%. The samples were prepared by thoroughly mixing Cu and Zn powders and alloying in a quartz tube in Ar atmosphere. Finally the samples were shaped as cylinders of 10-mm diameter. Analytical grade Zn powder (Merck) and purified Cu powder (J. T. Baker) were used in these experiments. In addition to the brass samples, aluminum, iron (technical alloy), and soil were analyzed for plasma propagation measurements. Soil samples were locally collected and pelletized at a pressure of 10 KPsi.

RESULTS AND DISCUSSION

Spatial Distribution of Plasma vs Time. We first explain the possibility of exchanging temporal gating by spatial resolution, by presenting the spatial distribution of the plasma at a series of delay times. Figure 2 shows a series of multidimensional spectral presentations. Each of them shows the spectra as a function of distance from the surface. (Note that in these measurements the light from all optical fibers were transferred to the ICCD detector and was gated. In the following measurements, the same seven optical fibers was connected to the CCD and not temporally gated.) In all cases the plasma was produced on a brass sample surface. Each such presentation was obtained for a given delay time after

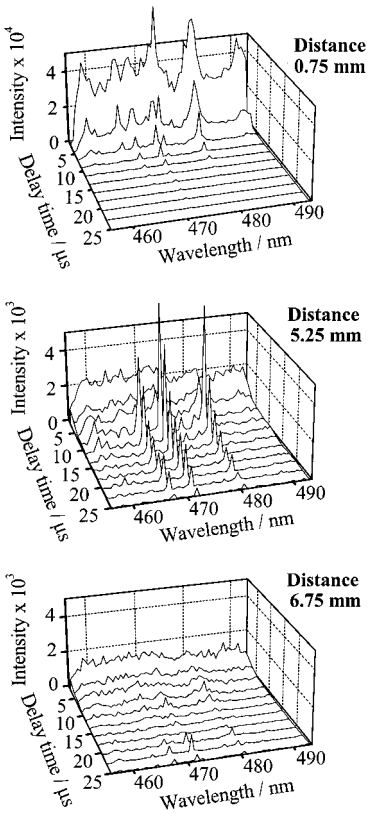

Figure 3. Spectra of brass sample vs delay time, acquired at the several distances from the surface. The integration time was 100 ns.

the laser shot. It can be seen that at a short delay (0.5 μs) the intense spectra are very close to the surface and no signal is observed at higher distances. The plasma is just created, and it has not propagated yet away from the surface. The temperature is high, resulting in intensive and broad spectra, with considerable background. Analysis performed at such delay times resulted in poor detectability.

At longer delays, the signals are weaker (note the different vertical scale in each panel) and they originate from longer distances from the surface. The propagation of plasma can be easily observed and measured from these figures. After 20 μs, the maximum emission intensity reaches a distance of 5.25 mm from the surface.

Additional information can be obtained by the temporal resolution of the spectra, observed at several locations along the plasma. Figure 3 shows the spectra as a function of time, observed at three different distances from the sample surface. It can be seen that when observing the plasma event from a position close to the surface, very intense spectra are recorded at the beginning, which then rapidly decay (in about 3 μs). Again, the intense spectra are not useful for analytical applications. Observation of the same event from a greater distance (5.25 mm) shows different characteristics: At the beginning, almost no spectra are observed. After some 7 μs, the plasma wave reaches the observation point and the signals increases. Then, they decrease again when the plasma continues to propagate and cools. It should be noted that the maximum intensities observed here are absolutely lower that those observed close to the surface; however, these spectra are much better for analytical purposes. At a larger distance (e.g. at 6.75 mm, bottom of figure), the signal reaches the observation point at a too long time, when the plasma is already cooled and the intensities are too low for reasonable spectral analysis.

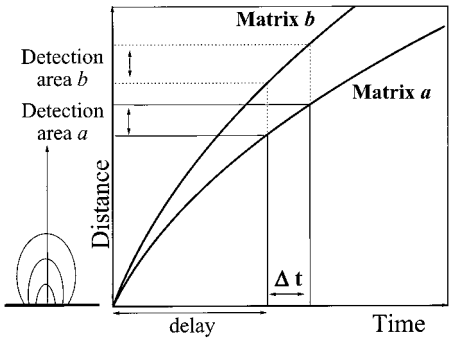

Figure 4. Schematic drawing explaining the basis of the exchange of the delay and integration times by spatial resolution.

A schematic presentation of the plasma front propagation and its application for converting spatial to temporal resolutions is shown in Figure 4. (This schematic figure is used for explanation of the principle; real data for several real matrixes and experimental conditions will be shown later.) The plasma front propagation is shown for two different matrixes. If a certain delay, *t*, and integration time, Δt, is needed, one can find a proper observation point and observation resolution which match this timing. However, the detection distance and area, which fit to a certain delay and integration time, are matrix dependent, as clearly seen in the above figure. In the following we present real results obtained from various matrixes; however, this schematic figure points out how the spatial resolution serves as temporal gating. Quantitative evaluation required a more detailed investigation of the plasma propagation, as described in the following.

Clearly, for a given matrix, observing the plasma perpendicularly to the laser beam and at a narrow sold angle corresponds to a certain delay and integration time. This is the principle of our conversion of spatial to temporal gating, as will be detailed in the following.

Propagation of Plasma. More accurate and detailed information on propagation of the plasma front was obtained using a PMT detector, tuning the spectrograph to a strong spectral line of an element of interest. Again, the spatial resolution was obtained by positioning the collecting optical fiber parallel to the plasma propagation vector, at various distances. Representative results of the plasma emission intensities as a function of time, obtained from a brass (90% Cu) sample, are shown in Figure 5. A sequence of emission maxima is observed, corresponding to the passing of the plasma wave in front of the measuring optical fiber. Normalized data are presented, since the emission intensities vary by several orders of magnitude when changing the observation point.

The results of Figure 5 indicate the feasibility of obtaining temporal gating from spatial resolution. Actually, measurement of plasma emission at distances of 2.25 and 3.75 mm, for example, is equivalent to gating measurements with integration time of about 3 μs and delay time of 0.75 and 2.5 μs correspondingly.

The description of the maxima of Figure 5 as a function of time is of considerable analytical interest. Figure 6 shows the distance (along the plasma propagation vector) as a function of the front arrival time. These plots characterize the plasma propagation and are matrix dependent. Actually, they provide an important physical characterization of the matrix, in terms of the

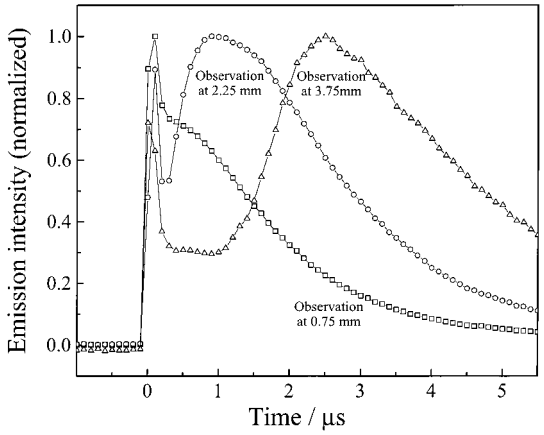

Figure 5. Oscilloscope diagrams of normalized emission intensities (Cu line at 324.7 nm) detected at several distances from a brass surface.

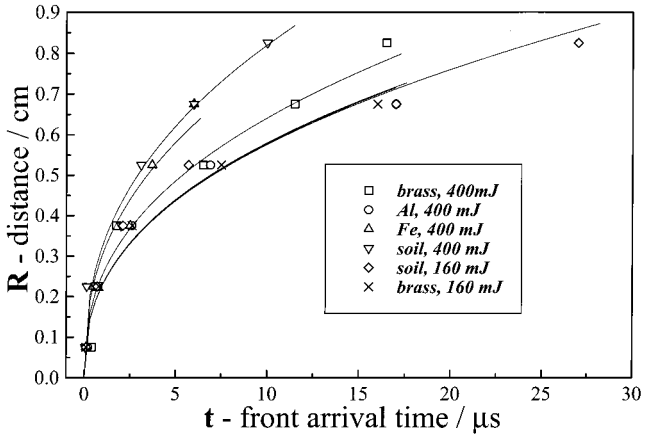

Figure 6. Axial distance of the maximum emission of plasma propagation, as a function of time. Results depend on material and laser pulse energy: symbols, experimental results; curves, fitting by expression (2).

laser-induced plasma profile. The first important observation is that the plots of Figure 6 are not linear, indicating a first accelerated propagation, followed by moderate stabilization of the plasma velocity. The second observation is that the velocity profile is matrix dependent. A more detailed analysis of these findings requires introduction of the shock-wave propagation theory. The concepts required in this presentation are briefly discussed in the following.

It is well-known that breakdown occurs as a result of the interaction of intense radiant flux with a medium. For gases, such intense fluxes can be obtained by focusing a laser beam; however, the breakdown threshold is extremely reduced on surfaces. The laser breakdown process and the followed shock wave propagation have been extensively studied since the Q-switch laser development. The physical backgrounds of these processes were reviewed,[34−35] and continued investigation is still under process.[36−43] However, mainly the physical point of view of shock-wave propagation was studied, while we are focused here on the analytical aspects of this process.

Our experimental setup excludes breakdown in air, and only surface breakdown takes place. We estimate the initial plasma plume size and show that laser ablation (under our experimental conditions) satisfies conditions of "point explosion", namely, a strong explosion in which a large amount of energy is liberated in a small volume (compared to the expansion volume). In this estimation we use a maximum velocity, which is the speed of laser detonation. This hydrodynamic mechanism is similar to the detonation of explosives.[44] This speed refers to the plasma propagation toward the laser source, when it is initially induced in air by a focused laser beam. The speed of the absorption wave can be calculated by the formula

$$D = \left[2(\gamma^2 - 1)\frac{G}{\varrho_0}\right]^{1/3} \qquad (1)$$

where D is the velocity of detonation, $\gamma = C_p/C_v$ ($\approx$1.4 for air), G is the laser beam energy flux, and ρ_0 is the normal air density (1.3×10^{-3} g cm^{-3}). In our typical experimental conditions, the pulse energy was 0.4 J, its duration was 7×10^{-9} s, and the beam diameter (on the surface) was 1.5 mm. Therefore, the estimated velocity of detonation is $D = 35$ km/s. (This is a reasonable laser detonation speed; in case of strong focusing, the velocity may reach 100 km/s.) At the end of the short laser pulse there still remains in the air a highly heated volume. (Its estimated size is less than 0.25 mm.) This volume expands, and the subsequent process is similar to that of a strong explosion in the atmosphere.

The heated gas and material in the absorbing layer expands and produces a shock wave in all directions, including that along the incoming laser beam. The gas is heated and ionized across the shock wave, so that a zone of light absorption and energy release is displaced behind the shock front.

The problem of a strong explosion in a homogeneous atmosphere is an example of a self-similar flow, in which the flow variables change in time in such a manner that their distributions regarding the coordinate variable always remain similar in time. The self-similar problem of a strong explosion was solved by Sedov.[45] Consider an ideal gas of constant specific heats and density ρ_0, in which a large amount of energy E is released in a small volume in a short time interval. Assume that the initial gas pressure can be neglected in comparison with the pressure behind the shock wave. The length scale of this event is represented by

(34) Ostrovskaya, G. V.; Zaidel, A. N. *Usp. Fiz. Nauk* **1973**, *111*, 579−615.
(35) Raizer, Ju. P. *Usp. Fiz. Nauk* **1980**, *132*, 549−581.
(36) Emmony, D. C.; Suaidi, M. K. B.; Ward, B. *Shock Waves at Marseile III: Shock waves in condensed matter and heterogeneous media*; Proceedings of the 19th International Symposium on Shock Waves, Marseile, France, July 26−30, 1993; Springer-Verlag: Berlin, New York, **1995**; pp 245−250.
(37) Kagawa, K.; Yokoi, S.; Nakajima, S. *Opt. Commun.* **1983**, *45*, 261−265.
(38) Gatti, M.; Palleschi, V.; Salvetti, A.; Singh, D. P.; Vaselli, M. *Opt. Commun.* **1988**, *69*, 141−146.
(39) Callies, G.; Berger, P.; Kaestle, J.; Huegel, H. In *International Symposium on Gas Flow and Chemical Lasers, 10th*, Friedrichshafen, Germany, Sept 5−9, 1994, Proceedings. *SPIE Proc.* **1995**, *2502*, 706−711.
(40) Jeong, S. H.; Greif, R.; Russo, R. E. *Appl. Surf. Sci.* **1998**, *127−129*, 1029−1034.
(41) Chen, K. R.; Leboeuf, J. N.; Wood, R. F.; Geohegan, D. B.; Donato, J. M.; Liu, C. L.; Puretzky, A. A. *Phys. Rev. Lett.* **1995**, *75*, 4706−4709.
(42) Angleraud, B.; Girault, C.; Champeaux, C.; Garrelie, F.; Germain, C.; Catherinot, A. *Appl. Surf. Sci.* **1996**, *96−98*, 117−121.
(43) Kurniawan, H.; Nakajima, S.; Batubara, J. E.; Marpaung, M.; Okamoto, M.; Kagava, K. *Appl. Spectrosc.* **1995**, *49*, 1067−1072.
(44) Zeldovich, Ya. B.; Raizer, Yu. P. *Physics of Shock Waves and High-Temperature Hydrodynamic Phenomena*; Academic Press: New York, 1966; Vol. 1.
(45) Sedov, L. I. *Similarity and Dimensional Methods in Mechanics*; Academic Press: New York, 1959.

Table 1. Comparison of the Experimental and Calculated Coefficient k for a Variety of Matrixes and Pulse Energies

sample	E_0, laser pulse energy (mJ)	k (cm/s$^{2/5}$) expl	k (cm/s$^{2/5}$) calcd
brass	400	65.02 ± 2.1	83.8
brass	160	58.0 ± 1.5	66.3
soil	400	82.0 ± 3.0	83.8
soil	160	57.6 ± 2.2	66.3
aluminum	400	57.8 ± 2.7	83.8
iron	400	76.7 ± 3.8	83.8

the radius of a sphere $R_0 = (E/\rho_0)^{1/3}$. The initial energy, E, is comparable to the explosion energy or to the laser pulse energy in our case. One finds that, under our experimental conditions, $R_0 \approx 1.5$ cm. The time scale is given by the time needed to a sound wave to travel this distance: $t_0 \approx 40$ μs.

In this model a shock wave propagates in the gas, starting from the point where the energy is released. The propagation of the wave front is described by the following expression:[44]

$$R = \xi_0\left(\frac{E}{\rho_0}\right)^{1/5} t^{2/5} \qquad (2)$$

Here R is the distance from the starting point, t is time, and ξ_0 is a dimensionless parameter, which is determined from energy conservation condition and depends on the specific heat capacity ratio γ ($\xi_0 = 1.033$ for $\gamma = 1.4$).

The above equation can be compared to our experimental results on plasma expansion. Actually, the R and t variables are exactly those shown in Figure 6. We fitted the experimental data to a function of the form $R = kt^{2/5}$. The solid curves in this figure show these functions, which are in good agreement with the observed experimental data. The free coefficient is obviously $k = \xi_0(E_0/\rho_0)^{1/5}$. In an ideal case it depends only upon the laser pulse energy E_0; however, it is not surprising that it is somewhat matrix dependent: the above-described simple model assumes coupling all laser energy into the plasma and does not consider the energy losses to the matrix. The model is also assumes plasma expansion in air and ignores the solid matrix and geometrical effects due to its particulate nature.

Actually, one can calculate the k values for the laser energy applied in these experiments and compare them with the fitting parameters of Figure 6. The calculated values are in reasonable agreement with the experimental ones; however, deviations more than the estimated errors are observed. The comparison is shown in Table 1.

A possible explanation of the observed slight discrepancy is that matrix effects are not properly included in this simple model. Actually, due to matrix effects, a portion of the laser light is not available for the shock-wave expansion: some of the energy may be reflected by the surface of the sample and/or dissipated to direct heating the surface. Another explanation is that the time variable in the experiment is not exactly the same as in the calculation: we detect the arrival time of the maximum emission of the evaporated materials, whereas the time in the model represents the propagation of the shock wave front. The expansion of the evaporated materials is affected by the dynamics of the evaporation process and by geometrical factors, such as local particulate size and spatial distribution of temperature. Note also that when soil samples are concerned, the mass of the evaporated material (about 100 μg; see ref 33) is comparable to the mass of the expanded atmospheric gases (about 650 μg for a 1 cm sphere). Therefore, the arrival time of the maximum emission and that of the shock-wave front may not exactly coincide.

Spatial Resolution vs Temporal Gating. The concept of exchanging the expensive temporal gating with nonexpensive spatial resolution was examined by LPS analysis of a series of brass samples. This material was chosen since its LPS analytical performance is well-known. Due the simplicity of these measurements, we avoid many of the matrix-related problems and we isolate the issue of interest, namely the comparison of the two methods.

The spectrometer was tuned to the range of 455−495 nm, which includes intense atomic lines of both Zn (472.22 and 481.05 nm) and Cu (458.69 and 465.11 nm).[46,47] Most LPS analyses utilize internal calibration based on the ratio of spectral lines, when the concentration of one element is constant. Actually, this procedure is not possible in most cases, including our case where no constant concentration is available. Therefore, we adopt here a different internal calibration procedure that has been recently proposed.[33] It is based on the finding that the same fluctuation patterns observed in the spectral peaks are present in the background intensity as well. On these grounds, the background intensity emission is applied as internal standard. This internal calibration method was proven to provide improved results; therefore, it is applied in this study as well. The exact procedure is described in the literature[33] and will be referred here as "signal to background" technique. Other similar internal calibration procedures are also known.[3,31]

First, we present the *absolute* LPS intensities, namely, the spectral peak areas (Figure 7). Calibration plots of Zn in brass are shown for a wide concentration range. This figure compares the traditional gated measurements to spatially resolved nongated results. The nongated calibration plots are presented for 7 distances from the surface, as previously described.

The main finding shown in this figure is that one can obtain a proper calibration plot at each distance from the surface, using a nongated setup. Obviously, the measurements at high distances result in small slopes, and poor sensitivity is expected. The highest signal is observed at a distance of 1.5 mm from the surface, where good sensitivity is obtained for a wide concentration range. Actually, when considering the spectral intensities and the slope of the calibration plots, best results are obtained from the nongated measurements. It means that nongated measurements obtained at a certain spatial location, perpendicular to the plasma propagation vector, are advantageous over traditional temporal gating. Measurements obtained at a distance of 4.5 mm result in a calibration plot, which is similar to that obtained at a delay of 4 μs and integration time of 2 μs.

Somewhat different figures are obtained when the signal-to-background technique is applied. As previously mentioned this technique (or similar internal calibrations) is often applied for compensating for signal variations. The experimental results are

(46) Zaidel, A. N.; Prokofiev, V. K.; Raisky, S. M.; Slavnyi, V. A.; Schraider, E. Ya. *Tables of Spectral Lines*; Nauka: Moscow, 1977.
(47) Moore, C. E. *Atomic Energy Levels*, National Bureau of Standards, Washington, DC, 1952; Circular NBS 467.

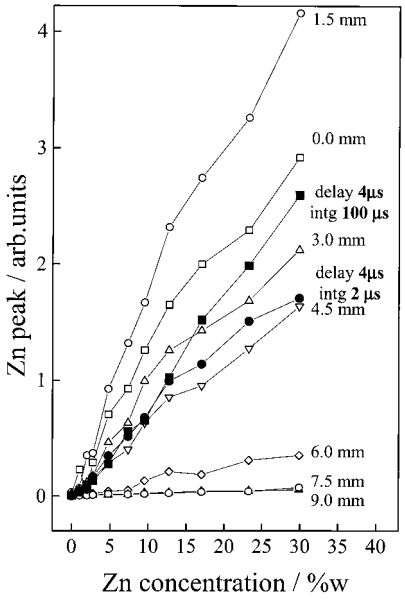

Figure 7. Calibration plots for Zn in brass, obtained in gated (solid marks) and in nongated experiments, at various distances. Note that best results are obtained with the nongated setup, at a proper spatial resolution.

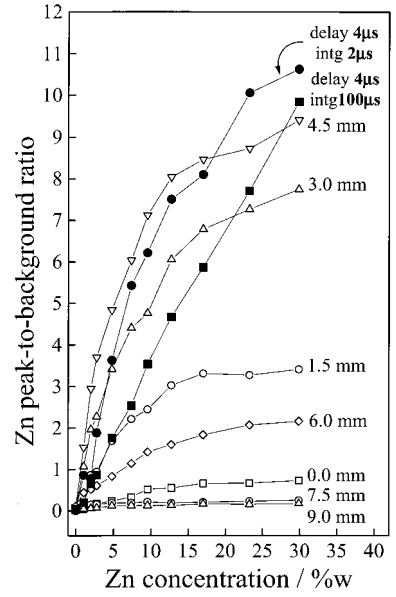

Figure 8. Same calibration plots as in Figure 7, however, based on the signal-to-background ratio. Note that despite the saturation-like behavior, best sensitivity is obtained with the nongated setup, at a distance of 4.5 mm (up to 17% Zn).

shown in Figure 8. Again, both the gated and the nongated results are presented together. Generally, the nongated results obtained at a specific location provide calibration plots that are comparable to those obtained in the gated experiments, over a wide concentration range (however, not over the full range).

Several observations can be pointed out, regarding the results of Figure 8: (a) Linear calibration curves are defined for all nongated analyses, in a certain concentration range (the saturation-like behavior at high concentrations will be discussed). (b) The slopes of the calibration plots depend on the observation point. They are low at extreme distances and reach a maximum at 4.5 mm. Note that at this particular distance, the sensitivity is even higher than that obtained in the best gated measurement. (c) The calibration plot at 100 μs integration time is more linear than at 2 μs, since the longer integration allows for averaging over nonlinearities which show up at certain times during plasma propagation. On the other hand, the signal-to-background ratio is higher at 2 μs integration time. The reason is that when a long integration time is applied, the detector accumulates more noise, which adds to the background. (d) The final significant observation is the general shape of the calibration curves obtained at the nongated experiments, namely, the saturation-like behavior. A certain saturation level is well-known for such high concentrations;[18] however, it seems that this effect is more pronounced here. The explanation is based on our previous matrix effects investigation.[32] As previously reported, the signal-to-background ratio corresponding to the main matrix constituents must undergo saturation at high concentrations. Here, as the concentration of Zn increases, it reaches the status of a matrix component and its signal-to-background ratio reaches the saturation regime.

When complex matrixes are concerned, there is no wavelength window free of weak spectral lines of the matrix elements. As a result, the background in laser plasma spectroscopy always contains a spectral component of the matrix itself. Therefore, the ratio of the signal of an element included in the matrix to the background must possess a saturation-like behavior. However, no such saturation is expected for trace elements, since their contribution to the background is truly negligible.

The main conclusion obtained from Figure 8 is that one can find a proper observation point where the nongated calibration plot is comparable to the one obtained by a gated setup. (In our measurements, a certain observation point provided slightly better results.) However, the advantage of the proposed setup is more pronounced when the absolute signal, rather than the signal-to-background, is used for calibration.

In this study we revealed a problem which was not properly emphasized in traditional LPS analysis, using gated detectors. It is related to the fact that the distribution of sampled materials in time and space actually depends on the individual element analyzed. The differences in the spatial distribution of Cu and Zn in the plasma were recently reported.[25] Therefore, the ratio of spectral intensities of various elements *does* depend on the time of measurement in the gated setups. This point is important since the internal calibration method, based on the ratio of spectral peaks, is routinely performed in PLS measurements. Erroneous results are expected when changing the gating characteristics or when adjusting the gating to an element of interest. We shall explain this point and the advantage of the nongated method in Figure 9.

Figure 9 shows the ratio of the spectral peaks of Zn and Cu as a function of distance from the surface, measured at various sample concentrations. These measurements were repeated three times: Using the nongated mode and using the gated setup (4 μs delay and 100 μs integration; 4 μs delay and 2 μs integration). Note that in the later mode we performed simultaneous gating of all optical fibers, inspecting the plasma at various distances.

Figure 9a shows the nongated measurements. Clearly, a monotonic increase of the Zn/Cu ratio is observed as the Zn concentration increases. Moreover, when the sample concentration is kept constant, the ratio increases monotonically with the

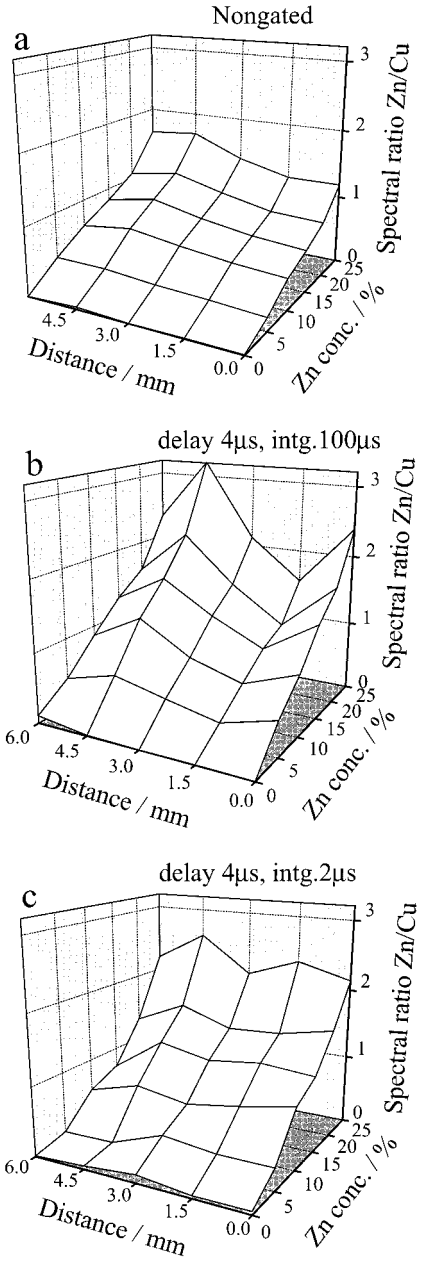

Figure 9. Spectral Zn-to-Cu ratio as a function of both observation distance and concentration: (a) nongated experiments; (b) 4 μs-delay time, 100 μs integration time; (c) 4 μs delay time, 2 μs integration time.

distance from surface. This finding is easily understood in terms of the explanation provided in ref 33, on the basis of the fact that the boiling point of Zn is lower than that of Cu and the former is more likely to be found at higher distances. (We compare the vapor pressure of the two compounds: At the fixed temperature, e.g., 900 °C, the vapor pressure of Zn is 12 orders of magnitude higher than that of Cu. Therefore, Zn evaporates first and predominantly expands into the external shell of the laser plume.) However, when gating the measurement and integrating over 100 μs, one finds a different situation, as shown in Figure 9b. The Zn/Cu ratio first decreases with distance and reaches a minimum at 1.5 mm. Then, it increases again until 5 mm above surface and decreases at 6 mm. A different behavior is observed at other timing, as shown in Figure 9c. When shortening the integration time to 2 μs, one observes a nonsystematic behavior of the Zn/Cu ratio up to 4.5 mm. (Although the S/N ratio is smaller in this case, it is still sufficient and the results are significant.) The actual ratio depends on both Zn concentration and distance. The complicated nature of this behavior is attributed to the fact that, at short integration times, results are very sensitive to the details of the dynamics of plasma propagation. The plasma expansion is a complicated function of both time and space, and no stable results are observed at snapshots. Since no detailed information on the plasma dynamics on this time scale is currently available, we cannot provide an explanation to the observed details. However, these kind of data could be found useful for development of plasma models.

As previously mentioned, more systematic information is observed when integrating over 100 μs and even better at the nongated measurements. These findings point out that long integrated and nongated LPS analyses may perform better, when the ratio of spectral lines is applied as an internal standard.

CONCLUSION

A method for performing LPS analysis, without expensive temporal resolution, was suggested and evaluated using a simple case study of brass samples. The method is a result of the investigation of plasma propagation in time and space. The main conclusion of this research is that spatial resolution in plasma analysis, obtained by an optical fiber placed perpendicular to the plasma propagation vector, can exchange the temporal gating. A multifiber setup coupled to an imaging spectrometer can provide the above information that corresponds to a series of time-gating conditions.

The signal-to-background ratios obtained this way were comparable to those obtained using a gated detector. It should be noted that this low-cost temporal resolution is achieved with no intrinsic limitation of the spectral resolution. The main advantage of the proposed setup is its simplicity and low cost; however, additional benefits were pointed out as well. It seems that application of the internal calibration technique may provide better results using the nongated technique.

Despite its apparent advantages, it should be pointed out that better analytical performance could probably be obtained with a gated device, provided that gating optimization is carried out. Therefore, when best results are needed, and one can afford the time required for gating optimization, the traditional method is preferred. It should be noted, however, that a proper optimization is needed for each spectral line. Moreover, the matrix effects, which are considered the most serious obstacle in LPS analysis, are better handled by temporal gating (again, provided that a proper optimization is carried out). However, a certain level of matrix optimization is possible in the spatially resolved (nongated) mode as well. This issue is now under investigation.

ACKNOWLEDGMENT

This study was supported, in part, by the Israel ministry of the environment and by the James Franck Program for Laser Matter Interaction. V.B. is grateful for financial support by Ministry of Absorption for new immigrant scientists.

Received for review February 9, 2000. Accepted March 26, 2000.

AC0001737